The Journal of Chemical Physics

Coherent state mapping ring polymer molecular dynamics for non-adiabatic quantum propagations

Cite as: J. Chem. Phys. **147**, 214109 (2017); https://doi.org/10.1063/1.4995616
Submitted: 12 July 2017 . Accepted: 17 November 2017 . Published Online: 06 December 2017

Sutirtha N. Chowdhury, and Pengfei Huo

Coherent state mapping ring polymer molecular dynamics for non-adiabatic quantum propagations

Sutirtha N. Chowdhury and Pengfei Huo[a)]
Department of Chemistry, University of Rochester, 120 Trustee Road, Rochester, New York 14627, USA

(Received 12 July 2017; accepted 17 November 2017; published online 6 December 2017)

We introduce the coherent-state mapping ring polymer molecular dynamics (CS-RPMD), a new method that accurately describes electronic non-adiabatic dynamics with explicit nuclear quantization. This new approach is derived by using coherent-state mapping representation for the electronic degrees of freedom (DOF) and the ring-polymer path-integral representation for the nuclear DOF. The CS-RPMD Hamiltonian does not contain any inter-bead coupling term in the state-dependent potential and correctly describes electronic Rabi oscillations. A classical equation of motion is used to sample initial configurations and propagate the trajectories from the CS-RPMD Hamiltonian. At the time equivalent to zero, the quantum Boltzmann distribution (QBD) is recovered by reweighting the sampled distribution with an additional phase factor. In a special limit that there is one bead for mapping variables and multiple beads for nuclei, CS-RPMD satisfies detailed balance and preserves an approximate QBD. Numerical tests of this method with a two-state model system show very good agreement with exact quantum results over a broad range of electronic couplings. *Published by AIP Publishing.* https://doi.org/10.1063/1.4995616

I. INTRODUCTION

Accurately simulating quantum dynamics effects, including non-adiabatic electronic transitions and nuclear quantum effects in large-scale condensed phase systems, is one of the central challenges in modern theoretical chemistry.[1] Direct simulations of the exact quantum dynamics in these systems remains to be computationally demanding. It is thus ideal to develop trajectory-based approximate methods that scale linearly with respect to the nuclear degrees of freedom (DOF) while, at the same time, accurately describe electronic non-adiabatic dynamics and nuclear quantum effects.

Mixed quantum-classical (MQC) and semi-classical (SC) dynamics approaches have already been proved as promising methods that can accurately describe electronic non-adiabatic transitions. The widely used MQC methods include Ehrenfest dynamics, surface-hopping (SH) dynamics,[2–4] and the mixed quantum-classical Liouville (MQCL) equation.[5–9] The commonly used SC methods include semi-classical initial-value representation (SC-IVR) path-integral methods[10,11] and linearized path-integral dynamics.[12–14] All of these methods use classical trajectories to propagate the nuclear DOF, thus significantly reduce the computational cost. However, the classical description of the nuclear dynamics causes inconsistencies between quantum and classical mechanics in MQC-based methods[15] and cannot preserve the quantum initial distribution such as the Wigner distribution used in SC-based methods.[16] These deficiencies can lead to problems such as the breakdown of detailed balance[17,18] or zero-point energy (ZPE) leakage.[19,20]

Imaginary-time path-integral approaches, including centroid molecular dynamics (CMD)[21,22] and ring-polymer molecular dynamics (RPMD),[23,24] have been successfully developed and applied to investigate nuclear quantum effects and electronic non-adiabatic dynamics in large-scale simulations. In particular, RPMD, which resembles classical MD in an extended phase space, provides a convenient approach to compute quantum correlation functions and rate constants.[23] In these methods, nuclear quantum statistics are captured with the imaginary-time path-integral formalism, leading to a ring-polymer classical isomorphism that describes quantum Boltzmann distribution (QBD) in the extended classical phase space. The classical evolution preserves the QBD captured by the ring-polymer Hamiltonian due to the symplectic nature of classical dynamics and will be free of the zero-point energy leakage problem. Despite its success in describing quantum effects in condensed phase, RPMD is limited to one-electron non-adiabatic dynamics[25] or nuclear quantization,[23] as well as the lack of the real-time electronic and nuclear coherence effects.[25]

Recent efforts have been focused on developing RPMD approaches with electronic-state representation, with a vision to accurately describe electronic dynamics and, at the same time, preserve QBD.[1] Unfortunately, such methods are still missing in the current literature. For example, the Mean-field RPMD (MF-RPMD) approach[26,27] preserves QBD; kinetically constrained RPMD (KC-RPMD)[28] preserves an approximated distribution that is close to QBD. However, they cannot properly describe electronic coherence because they do not contain explicit electronic-state information. The mapping-variable RPMD (MV-RPMD)[29] approach does employ explicit electronic-state variables and preserves the exact QBD, but it cannot accurately capture Rabi oscillations in a bare two-state

[a)]Electronic mail: pengfei.huo@rochester.edu

system.[1] On the other hand, mapping CMD,[30] ring-polymer surface-hopping (RPSH),[31,32] ring-polymer Ehrenfest dynamics,[33] and non-adiabatic mapping RPMD (NRPMD)[34] are promising methods to provide explicit and accurate electronic dynamics. However, these approaches usually lack rigorous derivations, and they do not preserve detailed balance in general.

In this paper, we rigorously derive a state-dependent ring-polymer Hamiltonian. Based on that, we develop a new RPMD approach, coherent-state mapping RPMD (CS-RPMD). Using the Meyer-Miller-Stock-Thoss (MMST)[35–37] representation in the coherent-state basis, we introduce continuous fictitious phase space variables (mapping variables) to represent the discrete electronic states. Applying the usual path-integral technique,[38–41] we derive the CS-RPMD partition function expression that provides exact QBD through the extended phase space description. Initial distributions in the CS-RPMD are sampled from the classical dynamics of the CS-RPMD Hamiltonian. By using the coherent-state basis for the mapping variables, the CS-RPMD Hamiltonian does not contain any inter-bead coupling terms in the state-dependent mapping potential, leading to an accurate description of the electronic dynamics and correct Rabi oscillations. In the adiabatic limit and state-independent limit, CS-RPMD reduces back to the regular RPMD, just like any state-dependent RPMD approaches,[27–29] and thus rigorously preserves QBD under this limit. In a special case that there is only one bead for the mapping variables but still multiple beads for the nuclear DOF, we can rigorously prove that CS-RPMD satisfies detailed balance and preserves an approximate QBD. While the NRPMD approach assumes a Hamiltonian that closely resembles the CS-RPMD Hamiltonian,[34] the current work demonstrates a rigorous way to derive this Hamiltonian with a partition function that provides exact QBD, providing a solid theoretical foundation.

II. THEORY

We start with expressing the total Hamiltonian operator of the system as follows:

$$\hat{H} = \hat{T} + \hat{V}_0 + \hat{H}_e = \frac{\hat{\mathbf{P}}^2}{2M} + V_0(\hat{\mathbf{R}}) + \sum_{n,m=1}^{L} V_{nm}(\hat{\mathbf{R}})|n\rangle\langle m|, \quad (1)$$

where $\hat{T}$ is the nuclear kinetic energy operator, $\hat{\mathbf{P}}$ is the nuclear momentum operator, and M is the nuclear mass. $V_0(\hat{\mathbf{R}})$ is the state-independent potential operator, and $\hat{H}_e = \sum_{nm} V_{nm}(\hat{\mathbf{R}})|n\rangle\langle m|$ is the state-dependent potential operator (electronic part of the Hamiltonian), with L being the total diabatic electronic states.

To derive the CS-RPMD Hamiltonian, we start from the canonical partition function defined as $\mathcal{Z} = \mathrm{Tr}_{\mathrm{en}}[e^{-\beta\hat{H}}]$, where $\mathrm{Tr}_{\mathrm{en}} = \mathrm{Tr}_{\mathrm{e}}\mathrm{Tr}_{\mathrm{n}}$ represents the trace over both electronic and nuclear DOF, $\beta = 1/k_{\mathrm{B}}T$ is the reciprocal temperature, and $\hat{H}$ is the total Hamiltonian operator defined in Eq. (1). The partition function can be exactly evaluated as $\mathcal{Z} = \mathrm{Tr}_{\mathrm{en}} \prod_{\alpha=1}^{N}[e^{-\beta_N\hat{H}}]$, with α as the imaginary-time (bead) index, and a higher effective temperature defined as $\beta_N = \beta/N$. Further splitting the Boltzmann operator by the Trotter expansion under the infinite bead limit $N \to \infty$ gives $\mathcal{Z} = \lim_{N\to\infty} \mathrm{Tr}_{\mathrm{en}} \prod_{\alpha=1}^{N}[e^{-\beta_N(\hat{T}+\hat{V}_0)}e^{-\beta_N\hat{H}_e}]$. Inserting N copies of the resolutions of identity $\hat{I}_{\mathbf{R}} = \int \mathbf{dR}_\alpha|\mathbf{R}_\alpha\rangle\langle\mathbf{R}_\alpha|$ and $\hat{I}_{\mathbf{P}} = \int \mathbf{dP}_\alpha|\mathbf{P}_\alpha\rangle\langle\mathbf{P}_\alpha|$, and explicitly performing the trace over the nuclear DOF based on the standard path-integral technique,[38–41] we have

$$\mathcal{Z} = \lim_{N\to\infty} \int d\{\mathbf{P}_\alpha\}d\{\mathbf{R}_\alpha\}e^{-\beta_N H_{\mathrm{rp}}}\mathrm{Tr}_{\mathrm{e}} \prod_{\alpha=1}^{N}[e^{-\beta_N\hat{H}_e(\mathbf{R}_\alpha)}], \quad (2)$$

with $\int d\{\mathbf{P}_\alpha\}d\{\mathbf{R}_\alpha\} = \prod_{\alpha=1}^{N}\int d\mathbf{P}_\alpha d\mathbf{R}_\alpha$. Here, the ring-polymer Hamiltonian H_{rp} is expressed as follows:

$$H_{\mathrm{rp}} = \sum_{\alpha=1}^{N} \frac{\mathbf{P}_\alpha^2}{2M} + V_0(\mathbf{R}_\alpha) + \frac{M}{2\beta_N^2\hbar^2}(\mathbf{R}_\alpha - \mathbf{R}_{\alpha-1})^2, \quad (3)$$

and the state-dependent potential operator $\hat{H}_e(\mathbf{R}_\alpha) = \sum_{n,m} V_{nm}(\mathbf{R}_\alpha)|n\rangle\langle m|$ parametrically depends upon α_{th} bead's nuclear position $\mathbf{R}_\alpha$.

The above partition function is a common expression and the starting point for all state-dependent RPMD approaches[26–29,34] and path-integral Monte Carlo (PIMC) methods.[42–45] The only difference among these approaches arises from the treatment of the electronic potential term $\mathrm{Tr}_{\mathrm{e}} \prod_{\alpha=1}^{N}[e^{-\beta_N\hat{H}_e(\mathbf{R}_\alpha)}]$. For example, in the mean-field RPMD approach,[26,27] the electronic potential is obtained from a weighted average of ring polymers in different electronic configurations; in the KC-RPMD approach,[28] the potential is obtained from the averaged ring-polymer kink configurations; in the MV-RPMD[29] approach, the electronic states are explicitly described with mapping variables in the Wigner representation;[46] in the NRPMD[34] approach, the electronic states are described with mapping variables in both position and momentum bases.

A. Mapping representation for electronic states

We use the Meyer-Miller-Stock-Thoss (MMST)[35–37] mapping representation to transform the discrete electronic states into continuous variables. Based on this representation, L diabatic electronic states are mapped onto L harmonic oscillators' ground and first excited states with the following relation: $|n\rangle \to |0_1 \ldots 1_n \ldots 0_L\rangle = \hat{a}_n^\dagger|0_1 \ldots 0_n \ldots 0_L\rangle$. Here, $|n\rangle$ is the diabatic state, and $|0_1 \ldots 1_n \ldots 0_L\rangle$ is the singly excited oscillator (SEO) state with $L-1$ oscillators in their ground states and the n_{th} oscillator in its first excited state. Thus, the MMST formulation provides the mapping relation $|n\rangle\langle m| \to \hat{a}_n^\dagger\hat{a}_m$, with $\hat{a}_n^\dagger = 1/\sqrt{2\hbar}\,(\hat{q}_n - \mathrm{i}\hat{p}_n)$ and $\hat{a}_m = 1/\sqrt{2\hbar}\,(\hat{q}_m + \mathrm{i}\hat{p}_m)$ as the creation and annihilation operators for the harmonic oscillator. With the MMST mapping representation, the state-dependent potential operator in Eq. (1) is transformed to

$$\sum_{n,m} V_{nm}(\mathbf{R}_\alpha)|n\rangle\langle m| \to \sum_{n,m} V_{nm}(\mathbf{R}_\alpha)\hat{a}_n^\dagger\hat{a}_m. \quad (4)$$

Using the above mapping relation, we can rewrite the partition function as

$$\mathcal{Z} = \lim_{N\to\infty} \int d\{\mathbf{P}_\alpha\} d\{\mathbf{R}_\alpha\} e^{-\beta_N H_{\rm rp}} \mathrm{Tr}_{\rm e} \prod_{\alpha=1}^{N} \left[e^{-\beta_N \sum_{nm} V_{nm}(\mathbf{R}_\alpha) \hat{a}_n^\dagger \hat{a}_m} \right]. \tag{5}$$

To proceed, we need to choose a convenient basis to evaluate the operators $\hat{a}_n^\dagger$ and $\hat{a}_m$ inside $\mathcal{Z}$. Recall that coherent states $|\mathbf{p}, \mathbf{q}\rangle = |p_1 q_1, \ldots, p_n q_n, \ldots p_L q_L\rangle$ are the eigenstates of the creation and annihilation operators, with the following eigen equations:

$$\hat{a}_m |\mathbf{p}, \mathbf{q}\rangle = \frac{(q_m + i p_m)}{\sqrt{2\hbar}} |\mathbf{p}, \mathbf{q}\rangle, \ \langle \mathbf{p}, \mathbf{q}| \hat{a}_n^\dagger = \langle \mathbf{p}, \mathbf{q}| \frac{(q_n - i p_n)}{\sqrt{2\hbar}}, \tag{6}$$

where $\mathbf{q} \equiv \{q_1, \ldots, q_n, \ldots, q_L\}$ and $\mathbf{p} \equiv \{p_1, \ldots, p_n, \ldots, p_L\}$.

The overlap between the coherent-state basis and the diabatic basis can be expressed as follows:

$$\langle \mathbf{p}, \mathbf{q}|n\rangle = \langle \mathbf{p}, \mathbf{q}|0_1 \ldots 1_n \ldots 0_L\rangle = \frac{(q_n - i p_n)}{\sqrt{2\hbar}} e^{-(\mathbf{q}^{\rm T}\mathbf{q} + \mathbf{p}^{\rm T}\mathbf{p})/4\hbar},$$
$$\langle m|\mathbf{p}, \mathbf{q}\rangle = \langle 0_1 \ldots 1_m \ldots 0_L|\mathbf{p}, \mathbf{q}\rangle = \frac{(q_m + i p_m)}{\sqrt{2\hbar}} e^{-(\mathbf{q}^{\rm T}\mathbf{q} + \mathbf{p}^{\rm T}\mathbf{p})/4\hbar}. \tag{7}$$

B. Derivation of the CS-RPMD Hamiltonian

Expanding the exponential of electronic Hamiltonian operator in Eq. (5) up to the linear order of β_N, under the limit that $\beta_N \to 0$, we obtain an equivalent expression as follows:

$$\mathcal{Z} = \lim_{N\to\infty} \int d\{\mathbf{P}_\alpha\} d\{\mathbf{R}_\alpha\} e^{-\beta_N H_{\rm rp}} \times \mathrm{Tr}_{\rm e} \prod_{\alpha=1}^{N} \left[1 - \beta_N \sum_{nm} V_{nm}(\mathbf{R}_\alpha) \hat{a}_n^\dagger \hat{a}_m + \mathcal{O}(\beta_N^2) \right]. \tag{8}$$

To proceed, recall the commutation relationship between the creation and annihilation operators $\hat{a}_n^\dagger \hat{a}_m = \hat{a}_m \hat{a}_n^\dagger - \delta_{nm}$. Using this relation, Eq. (8) becomes

$$\mathcal{Z} = \lim_{N\to\infty} \int d\{\mathbf{P}_\alpha\} d\{\mathbf{R}_\alpha\} e^{-\beta_N H_{\rm rp}} \mathrm{Tr}_{\rm e} \prod_{\alpha=1}^{N} \times \left[1 - \beta_N \sum_{nm} V_{nm}(\mathbf{R}_\alpha) (\hat{a}_m \hat{a}_n^\dagger - \delta_{nm}) + \mathcal{O}(\beta_N^2) \right]. \tag{9}$$

Now by inserting N copies of the resolution of identity for the coherent state $I_{\mathbf{p},\mathbf{q}} = (1/2\pi\hbar)^L \int d\mathbf{p}_\alpha d\mathbf{q}_\alpha |\mathbf{p}_\alpha, \mathbf{q}_\alpha\rangle\langle \mathbf{p}_\alpha, \mathbf{q}_\alpha|$ in Eq. (9), and leaving out the higher-order terms $\mathcal{O}(\beta_N^2)$ under the $\beta_N \to 0$ limit, we have

$$\mathcal{Z} \propto \lim_{N\to\infty} \int d\{\mathbf{P}_\alpha\} d\{\mathbf{R}_\alpha\} e^{-\beta_N H_{\rm rp}} \int d\{\mathbf{p}_\alpha\} d\{\mathbf{q}_\alpha\} \times \mathrm{Tr}_{\rm e} \prod_{\alpha=1}^{N} \left[|\mathbf{p}_\alpha \mathbf{q}_\alpha\rangle\langle \mathbf{p}_\alpha \mathbf{q}_\alpha| - \beta_N \sum_{nm} V_{nm}(\mathbf{R}_\alpha) \times \left(\hat{a}_m |\mathbf{p}_\alpha \mathbf{q}_\alpha\rangle\langle \mathbf{p}_\alpha \mathbf{q}_\alpha| \hat{a}_n^\dagger - \delta_{nm} |\mathbf{p}_\alpha \mathbf{q}_\alpha\rangle\langle \mathbf{p}_\alpha \mathbf{q}_\alpha| \right) \right], \tag{10}$$

with $d\{\mathbf{p}_\alpha\} d\{\mathbf{q}_\alpha\} = \prod_{\alpha=1}^{N} d\mathbf{p}_\alpha d\mathbf{q}_\alpha$.

Further applying Eq. (6) to evaluate $\hat{a}_m$ and $\hat{a}_n^\dagger$, setting $\hbar = 1$ from now on, and inserting the diabatic projection operator $\mathcal{P} = \sum_n |n\rangle\langle n|$ in between the coherent-state basis to ensure correct projection onto the finite subspace of SEOs,[29,44] we obtain the following expression:

$$\mathcal{Z} \propto \lim_{N\to\infty} \int d\{\mathbf{P}_\alpha\} d\{\mathbf{R}_\alpha\} e^{-\beta_N H_{\rm rp}} \int d\{\mathbf{p}_\alpha\} d\{\mathbf{q}_\alpha\} \times \prod_{\alpha=1}^{N} \langle \mathbf{p}_\alpha, \mathbf{q}_\alpha| \sum_n |n\rangle\langle n|\mathbf{p}_{\alpha+1}, \mathbf{q}_{\alpha+1}\rangle \left\{ 1 - \beta_N \sum_{nm} V_{nm}(\mathbf{R}_\alpha) \times \left[\frac{1}{2} [\mathbf{q}_\alpha + i\mathbf{p}_\alpha]_m [\mathbf{q}_\alpha - i\mathbf{p}_\alpha]_n - \delta_{nm} \right] \right\}. \tag{11}$$

Based on a similar derivation procedure developed for the real-time propagator,[7,8] now we express the {third line} of the above expression back to the full exponential factor and explicitly evaluate the overlap between the coherent-state basis and the diabatic basis. We arrive at the final expression of the coherent-state partition function $\mathcal{Z}_{\rm cs}$ as the central result of this paper,

$$\mathcal{Z}_{\rm cs} \propto \lim_{N\to\infty} \int d\{\mathbf{P}_\alpha\} d\{\mathbf{R}_\alpha\} e^{-\beta_N H_{\rm rp}} \int d\{\mathbf{p}_\alpha\} d\{\mathbf{q}_\alpha\} \times \prod_{\alpha=1}^{N} \frac{1}{2} (\mathbf{q}_\alpha - i\mathbf{p}_\alpha)^{\rm T} (\mathbf{q}_{\alpha+1} + i\mathbf{p}_{\alpha+1}) e^{-\frac{1}{2}(\mathbf{q}_\alpha^{\rm T}\mathbf{q}_\alpha + \mathbf{p}_\alpha^{\rm T}\mathbf{p}_\alpha)} \times e^{-\beta_N \sum_{nm} V_{nm}(\mathbf{R}_\alpha) \left[\frac{1}{2} ([\mathbf{q}_\alpha]_m [\mathbf{q}_\alpha]_n + [\mathbf{p}_\alpha]_m [\mathbf{p}_\alpha]_n) - \delta_{nm} \right]}. \tag{12}$$

The above coherent-state partition function can be written in more compact form as follows:

$$\mathcal{Z}_{\rm cs} \propto \lim_{N\to\infty} \int d\{\mathbf{P}_\alpha\} d\{\mathbf{R}_\alpha\} \int d\{\mathbf{p}_\alpha\} d\{\mathbf{q}_\alpha\} \mathbf{\Gamma} e^{-\beta_N H_{\rm cs}}, \tag{13}$$

with the weighting factor

$$\mathbf{\Gamma} = \prod_{\alpha=1}^{N} \frac{1}{2} (\mathbf{q}_\alpha - i\mathbf{p}_\alpha)^{\rm T} (\mathbf{q}_{\alpha+1} + i\mathbf{p}_{\alpha+1}) e^{-\frac{1}{2}(\mathbf{q}_\alpha^{\rm T}\mathbf{q}_\alpha + \mathbf{p}_\alpha^{\rm T}\mathbf{p}_\alpha)} \tag{14}$$

and the CS-RPMD Hamiltonian

$$H_{\rm cs} = \sum_{\alpha=1}^{N} \frac{\mathbf{P}_\alpha{}^2}{2M} + V_0(\mathbf{R}_\alpha) + \frac{M}{2\beta_N^2 \hbar^2} (\mathbf{R}_\alpha - \mathbf{R}_{\alpha-1})^2 + \sum_{nm} V_{nm}(\mathbf{R}_\alpha) \left[\frac{1}{2} ([\mathbf{q}_\alpha]_m [\mathbf{q}_\alpha]_n + [\mathbf{p}_\alpha]_m [\mathbf{p}_\alpha]_n) - \delta_{nm} \right]. \tag{15}$$

The first line in $H_{\rm cs}$ corresponds to the nuclear ring-polymer part of the Hamiltonian, and the second line corresponds to the non-adiabatic part of the Hamiltonian which describes electron-nucleus interactions. Note that $H_{\rm cs}$ does not contain a potential that couples two adjacent mapping beads. A similar feature has also been proposed in the NRPMD Hamiltonian,[34] which ensures to capture the correct electronic Rabi oscillations. Here, we derived $H_{\rm cs}$ with this feature. To be specific, when the electronic DOF are decoupled from the nuclear DOF, such that $V_{nm}(\mathbf{R}_\alpha) = V_{nm}$, the non-adiabatic part of $H_{\rm cs}$ becomes the MMST Hamiltonian with bead-averaged initial conditions, which gives the exact frequency for electronic Rabi oscillations.[36,37] Meanwhile, MV-RPMD[29] does contain inter-bead coupling for mapping DOF and cannot capture the correct Rabi oscillations.[1]

We would like to emphasize several other key features of the CS-RPMD approach. First, CS-RPMD will reduce back to regular adiabatic RPMD with the decoupled electron-nucleus limit, including the state-independent limit $V_{nm} = 0$ $(n \neq m)$ and the adiabatic limit $\beta V_{nm} \gg 1$. Second, CS-RPMD has a very

clear one-bead limit. With only one bead for both mapping and nuclear DOF, the CS-RPMD Hamiltonian reduces back to the MMST mapping Hamiltonian in the coherent-state representation. Third, through a wick rotation, $\beta \rightarrow it/\hbar$, the coherent-state partition function $Z_{\rm cs}$ in Eq. (12) becomes a coherent-state real-time propagator used in the Forward-Backward MQCL (FB-MQCL) equation[7,8] and the Partial-Linearized Density Matrix (PLDM) approach.[14,47] In the FB-MQCL equation, the $\mathbf{\Gamma}$ term appears as the overlap between two coherent-state bases from two consecutive real-time propagators.[7,8]

We further emphasize that the possible mapping RPMD Hamiltonian expression is not unique, for instance, we have also obtained the MV-RPMD Hamiltonian in the coherent-state representation as presented in Appendix A. The reason for this non-uniqueness is that the quantum partition function in Eq. (2) is an integral of the function of the Hamiltonian; thus, it is mathematically possible to find a different Hamiltonian (integrand) that gives the same quantum partition function (integral).

C. CS-RPMD time correlation function

With the derived partition function [Eq. (13)] and $H_{\rm cs}$ [Eq. (15)], we *propose* to use them to compute the Kubo-transformed time correlation function for operators $\hat{A}$ and $\hat{B}$,

$$\tilde{C}_{AB}(t) = \frac{1}{\mathcal{Z}\beta}\int_0^\beta \mathrm{Tr}[e^{-(\beta-\lambda)\hat{H}}\hat{A}e^{-\lambda\hat{H}}e^{i\hat{H}t/\hbar}\hat{B}e^{-i\hat{H}t/\hbar}]d\lambda. \quad (16)$$

Similar to the original RPMD approach, we propose that the CS-RPMD correlation function,

$$C_{AB}(t) = \frac{1}{\mathcal{Z}_{\rm cs}}\int d\{\mathbf{R}_\alpha\}d\{\mathbf{P}_\alpha\}d\{\mathbf{q}_\alpha\}d\{\mathbf{p}_\alpha\}\mathbf{\Gamma}(0)e^{-\beta_N\hat{H}_{\rm cs}}\bar{A}(0)\bar{B}(t), \quad (17)$$

is an approximate Kubo-transformed time correlation function,[23,46] where $\bar{A}(0)$ and $\bar{B}(t)$ are the bead-averaged estimators for the corresponding operators. Note that $\mathbf{\Gamma}(0)$ in Eq. (14) is evaluated with the initial mapping variables at t = 0, and $\bar{B}(t)$ is evaluated with the classical trajectories generated from the Hamiltonian $H_{\rm cs}$. In this paper, we are interested in two types of auto-correlation functions: (1) nuclear position auto-correlation function $C_{RR}(t)$, where $\hat{A} = \hat{B} = \hat{R}$ and thus $\bar{A} = \bar{B} = \frac{1}{N}\sum_{\alpha=1}^N \mathbf{R}_\alpha$, and (2) population auto-correlation function $C_{nn}(t)$, where $\hat{A} = \hat{B} = |n\rangle\langle n|$ with the corresponding estimator

$$\bar{A} = \bar{B} = \frac{1}{N}\sum_{\alpha=1}^N \frac{[\mathbf{q}_\alpha - i\mathbf{p}_\alpha]_n[\mathbf{q}_{\alpha+1} + i\mathbf{p}_{\alpha+1}]_n}{(\mathbf{q}_\alpha - i\mathbf{p}_\alpha)^{\rm T}(\mathbf{q}_{\alpha+1} + i\mathbf{p}_{\alpha+1})}. \quad (18)$$

The CS-RPMD time correlation function can be computed by sampling initial configurations with NVT trajectories generated from $H_{\rm cs}$ and then propagating the dynamics with the same Hamiltonian H_{cs} to evaluate $\bar{B}(t)$. Each trajectory is weighted by an *initial* weighting factor $\mathbf{\Gamma}$ [Eq. (14)]. Note that both $\mathbf{\Gamma}$ and the projection operator estimator are complex. We thus use their complex values to accumulate the time correlation function. We obtain results of $C_{AB}(t)$ with zero complex values within numerical errors.

The novelty of the CS-RPMD formalism is that through the classical evolution of $H_{\rm cs}$, the initial configuration governed by $e^{-\beta_N H_{\rm cs}}$ is preserved for the ensemble of trajectories. Thus, CS-RPMD provides a stable propagation scheme for the dynamics and avoids initial configuration leakage problems. The NRPMD approach,[34] on the other hand, uses one Hamiltonian (that closely resembles the MV-RPMD Hamiltonian) to sample the initial configurations and another Hamiltonian (that closely resembles the CS-RPMD Hamiltonian) to propagate dynamics and thus might encounter the initial configuration leakage problem. Similarly, in commonly used linearized path-integral approaches (classical Wigner methods),[12–14,47] the classical nuclear propagation cannot preserve the Wigner initial distribution and might cause the zero-point energy leakage problem.[20] Just like any imaginary-time path-integral method, CS-RPMD uses classical dynamics in the extended phase space to quantize nuclei rather than initially enforce ZPE through the Wigner distribution, thus significantly alleviating the ZPE leakage problem encountered in the classical Wigner methods.[20]

However, CS-RPMD does not preserve QBD in general, despite the fact that the partition function in Eq. (13) exactly describes the QBD for any quantum statistics calculation (under the $N \rightarrow\infty$ limit for both nuclear and mapping variables). As can be clearly seen in Eq. (13), the CS-RPMD partition function requires an additional weighting factor $\mathbf{\Gamma}$ to be multiplied with $e^{-\beta_N H_{cs}}$ in order to recover QBD. This can be easily accomplished for quantum statistics calculations. On the other hand, for any time correlation function calculation, the pre-factor $\mathbf{\Gamma}$ [Eq. (14)] is not a constant during the classical evolution governed by $H_{\rm cs}$. Thus, CS-RPMD time correlation function calculations, which only use $\mathbf{\Gamma}(0)$ as an *initial* weighting factor, do not preserve QBD in general, especially at a longer time. As a consequence, CS-RPMD in general does not preserve ZPE associated with QBD, except at time $t = 0$, or under the adiabatic or state-independent limit. Despite this deficiency, our numerical results demonstrate that an accurate time correlation function can still be obtained. In the state-independent or the adiabatic limit, on the other hand, CS-RPMD reduces back to regular RPMD and preserves QBD, just like any state-dependent RPMD approaches.[29]

For a special case where there is only one bead for the mapping DOF (such that all mapping beads collapse into one), but still multiple beads for the nuclear DOF, $\mathbf{\Gamma} = \frac{1}{2}\sum_n(q_n^2 + p_n^2)e^{-\frac{1}{2}(\mathbf{q}^{\rm T}\mathbf{q}+\mathbf{p}^{\rm T}\mathbf{p})} = \langle\mathbf{pq}|\sum_n|n\rangle\langle n|\mathbf{pq}\rangle$ is indeed the integral of motion of $H_{\rm cs}$. Thus in this special case, CS-RPMD preserves detailed balance, such that[16,48] $C_{AB}(t) = C_{BA}(-t)$, with an approximate QBD generated from one mapping bead and N nuclear beads. Under this limit, the CS-RPMD Hamiltonian in Eq. (15) becomes $H_{\rm cs} = \sum_{\alpha=1}^N \frac{\mathbf{P}_\alpha^2}{2M} + V_0(\mathbf{R}_\alpha) + \frac{M}{2\beta_N^2\hbar^2}(\mathbf{R}_\alpha - \mathbf{R}_{\alpha-1})^2 + \sum_{nm} V_{nm}(\mathbf{R}_\alpha)\left[\frac{1}{2}(q_mq_n + p_mp_n) - \delta_{nm}\right]$, which is the ring-polymer nuclei under the coherent-state MMST potential. Note that the projection operator $\mathcal{P} = \sum_n|n\rangle\langle n|$ in the $\mathbf{\Gamma}$ expression constrains the electronic mapping variables within the physical SEO subspace.[44] This gives the partition function $\mathrm{Tr}[\mathbf{\Gamma}e^{-\beta_N H_{\rm cs}}]$ (with $\mathrm{Tr} \equiv \int \mathbf{dRdqdp}$) rather than simply assuming a classical partition function $\mathrm{Tr}[e^{-\beta_N H_{\rm cs}}]$.

In addition, CS-RPMD preserves Rabi oscillations as well as detailed balance under this special one-bead mapping limit. However, we need to emphasize that by using only one bead for the mapping variables, one cannot fully recover the exact QBD even at t = 0. In order to obtain the exact QBD [see Eq. (10)], we explicitly require $\beta_N \to 0$ (and $N \to \infty$) for both electronic and nuclear DOF in our derivations. Nevertheless, our numerical results (provided in Appendix C) suggest that the quantum statistics obtained from this approximated partition function is close to the exact QBD, and the time correlation function is close to both exact results and the CS-RPMD calculation with multiple beads for all DOF. We want to further emphasize that this limiting case has already proven to be useful in recently developed approaches, such as Ehrenfest RPMD[33] and RPSH,[31,32] which assume one bead for the electronic DOF and multiple beads for the nuclear DOF.

Finally, due to the presence of the MMST mapping Hamiltonian in $H_{\rm cs}$, extra caution is still needed. It is well known that this Hamiltonian could exhibit the "inverted potential" problem[49] when $\frac{1}{2}([q_\alpha]_n^2 + [p_\alpha]_n^2) - 1 < 0$ as well as the ZPE leakage problem associated with the mapping DOF due to the explicitly incorporated ZPE term, i.e., $-\sum_n V_{nn}(\mathbf{R}_\alpha)$. These intrinsic deficiencies associated with the MMST Hamiltonian can be addressed and refined with the recent theoretical developments, such as applying the semi-classical approximation to treat the mapping DOF,[14,50] using ZPE corrections for the mapping variables,[19,51] or using new forms of mapping Hamiltonians.[52,53]

D. Connections and differences with other methods

The CS-RPMD Hamiltonian is derived with the coherent-state basis for mapping variables, and it is closely related to two recently developed state-dependent RPMD formalisms: MV-RPMD[29] and NRPMD.[34] Here we want to clarify the connections and differences between CS-RPMD and these two methods.

First, the MV-RPMD Hamiltonian does contain inter-bead couplings for the mapping DOF[29] and cannot correctly capture the electronic Rabi oscillations in a bare two-state system.[1] In addition, the inter-bead couplings for mapping DOF in MV-RPMD might cause unphysical oscillation frequency even in the nuclear auto-correlation function calculations, as demonstrated in Sec. III. We further emphasize that the possible form of the state-dependent Hamiltonian that gives exact QBD for quantum statistics calculations is not unique. For instance, we can also obtain the MV-RPMD Hamiltonian[29] in the coherent-state representation, as presented in Appendix A. On the other hand, the MV-RPMD approach does preserve QBD throughout its dynamical propagation, which is an appealing feature.

Second, the NRPMD approach[34] uses a proposed Hamiltonian that closely resembles $H_{\rm cs}$ [Eq. (15)] to propagate dynamics and thus provides accurate electronic Rabi oscillations. However, the initial phase space points in this method are not sampled from the same Hamiltonian, but from another one that contains inter-bead coupling terms in the mapping potential.[34] By doing so, each trajectory in the NRPMD approach might move out of the original phase space distribution because of using two different Hamiltonians. Thus, NRPMD might encounter the initial configuration leakage problem. In the coherent-state basis context, this corresponds to a method that uses the coherent-state MV-RPMD Hamiltonian $H_{\rm cmv}$ [Eq. (A2) in Appendix A] to sample initial configurations and then uses CS-RPMD Hamiltonian $H_{\rm cs}$ [Eq. (15)] to propagate trajectories. Besides that, NRPMD also requires two estimators for the projection operator in order to efficiently compute the population correlation function.[34,54] The CS-RPMD approach, on the other hand, uses only one estimator [Eq. (18)].

Compared to these two recently developed mapping RPMD approaches, the merits of CS-RPMD are (1) preserving the electronic Rabi oscillations that MV-RPMD fails to describe, through a rigorously derived $H_{\rm cs}$ that does not contain any inter-bead coupling terms for mapping DOF, (2) sampling and propagating trajectories from one *derived* Hamiltonian, as opposed to the NRPMD approach that uses two Hamiltonians without rigorous derivations, and (3) preserving detailed balance with an approximate QBD in a special case that contains only one mapping bead.

However, we must admit that the numerical results obtained with CS-RPMD (for the current model systems) are not significantly different than those obtained from NRPMD. This suggests that both $H_{\rm cs}$ and the Hamiltonian proposed in NRPMD (which closely resembles $H_{\rm cs}$) provide accurate dynamics. While the NRPMD approach simply assumes a Hamiltonian of this form,[34] the current work demonstrates how to rigorously derive this Hamiltonian from a partition function that provides exact QBD.

III. RESULTS AND DISCUSSION

To test the accuracy of CS-RPMD, we adapt a commonly used model system that contains one nuclear coordinate and two electronic states,[29,34]

$$\hat{H} = \frac{\hat{P}^2}{2M} + \frac{1}{2}M\omega^2\hat{R}^2 + \begin{bmatrix} \epsilon + k\hat{R} & \Delta \\ \Delta & -\epsilon - k\hat{R} \end{bmatrix}, \tag{19}$$

where Δ is the electronic coupling, k is the vibronic coupling, and 2ϵ is the energy bias between the two diabatic states. In this paper, we choose a reduced unit system such that $M = \hbar = 1$ and $\omega = \beta = k = 1$.

Table I presents the parameters for all of the model systems used in this paper. In particular, models I and V are in the adiabatic regime, where $\Delta \gg \beta^{-1}$; models II and III are in the non-adiabatic regime, where $\Delta \ll \beta^{-1}$; models IV and VI are in the intermediate regime, where $\Delta \sim \beta^{-1}$. Models III and VI are asymmetric cases with finite diabatic energy bias 2ϵ, and the rest of the model systems are symmetric cases with $\epsilon = 0$.

TABLE I. Parameters (in a.u.) for model systems I-VI.

	I	II	III	IV	V	VI
ϵ	0	0	1.5	0	0	2
Δ	10	0.10	0.10	1	4	1

CS-RPMD correlation functions are computed from Eq. (17). To evaluate the ensemble average, a total number of 10^4 initial configurations are sampled from a 2×10^7 a.u. long CS-RPMD NVT trajectory, thermostatted by resampling the nuclear velocities from the Maxwell-Boltzmann distribution at every $0.4/\Delta$ a.u. Each configuration is then further equilibrated with NVE CS-RPMD propagation for another 200 a.u., before being used to propagate and accumulate the CS-RPMD correlation function. All of the correlation functions converge at $N = 8$ or fewer beads. Numerical exact results are obtained from discrete variable representation (DVR) calculations.[55]

Figure 1 presents the nuclear position auto-correlation function computed from CS-RPMD (black), the mean-field RPMD[26,29] approach (blue) with expression provided in Appendix B, and the numerical exact method (red) for models I-IV. Model I in Fig. 1(a) is in the adiabatic regime. In this case, CS-RPMD goes back to the standard RPMD and agrees with the exact result due to the near-harmonic adiabatic potential. Mean-field RPMD in this case also gives the same exact result and thus is not shown here. Model II in Fig. 1(b) is in the non-adiabatic regime. This is the most challenging case and the most relevant regime for non-adiabatic electron transfer[25] and proton-coupled electron transfer reactions.[56] In this regime, mean-field RPMD starts to break down even at a very short time. CS-RPMD, on the other hand, performs reasonably well compared to exact DVR calculations at a longer time. Models III and IV are in the intermediate regime, with asymmetric [Fig. 1(c)] and symmetric [Fig. 1(d)] diabatic bias 2ϵ. In this regime, both CS-RPMD and mean-field RPMD behave reasonably well.

We have also tested the special case when there is only one bead for mapping DOF, with the results provided in Appendix C. With $N = 8$ beads for the nuclear DOF and only one bead for the mapping DOF, we found good agreement for these correlation functions compared to the results obtained with multiple beads for all DOF, suggesting a promising practical strategy for preserving detailed balance as well as providing accurate non-adiabatic dynamics.

Figure 2 presents the comparison between CS-RPMD, NRPMD, and MV-RPMD. In Fig. 2(a), model I is used to illustrate the initial distribution leakage problem that NRPMD encounters. Here we present the results obtained from NRPMD[34] (blue), CS-RPMD (black), and the numerical exact method (red). In this adiabatic test case, all of the state-dependent RPMD approaches are expected to reduce to the regular RPMD approach and reproduce the exact result due to the nearly harmonic adiabatic potential in this model. This is indeed the case for MF-RPMD,[29] MV-RPMD,[29] and CS-RPMD, all of which can fully recover the exact result under this limit. However, as can be seen from Fig. 2(a), the result from the NRPMD approach starts to deviate from the exact one at longer times. This is due to the fact that in the NRPMD approach,[34] the Hamiltonian used to propagate trajectories will not preserve the initial distribution for the ensemble of trajectories that is sampled from another Hamiltonian. A similar situation is also encountered in the coherent-state version of NRPMD (result not shown) that samples initial configurations with $H_{\rm cmv}$ [Eq. (A2) in Appendix A] and propagates trajectories with $H_{\rm cs}$ [Eq. (15)]. CS-RPMD provides accurate long-time dynamics for this adiabatic test case, by sampling and propagating trajectories with the same Hamiltonian $H_{\rm cs}$ and thus preserving the phase space distribution for the ensemble of trajectories governed by $H_{\rm cs}$ throughout the dynamical propagation.

In Fig. 2(b), model II is used to provide the comparison between MV-RPMD and CS-RPMD. Here we present the

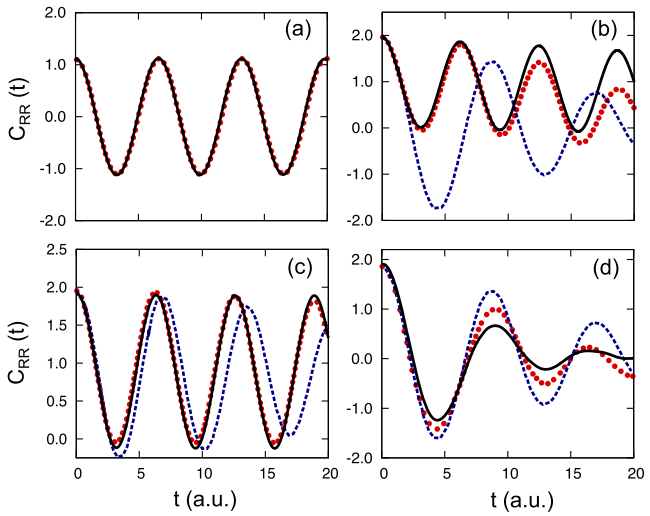

FIG. 1. The Kubo-transformed nuclear position auto-correlation function for models I-IV obtained from CS-RPMD (black solid lines), the mean-field RPMD (blue dashed lines), and numerical exact results (red dotted lines). Results for model I (symmetric, adiabatic) are in panel (a), model II (symmetric, non-adiabatic) are in panel (b), model III (asymmetric, non-adiabatic) are in panel (c), and model IV (symmetric, intermediate) are in panel (d).

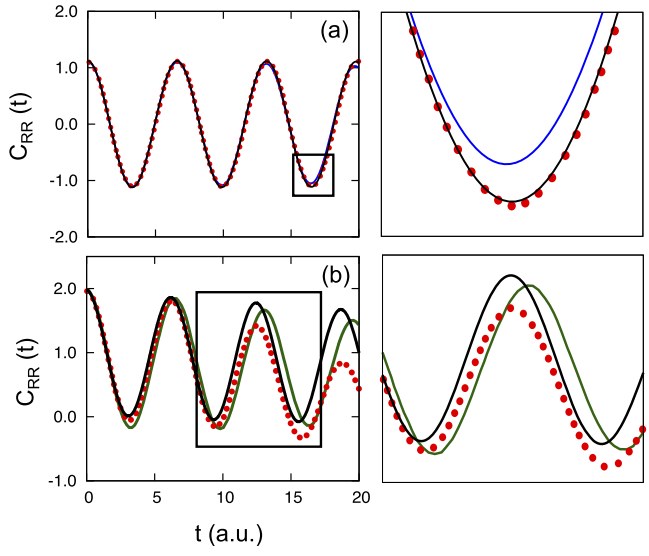

FIG. 2. Comparison between CS-RPMD and NRPMD[34] and MV-RPMD.[29] (a) The Kubo-transformed nuclear position auto-correlation function for model I obtained from CS-RPMD (black), NRPMD (blue), and numerical exact results (red). In this adiabatic case, MV-RPMD agrees with numerical exact results and thus is not shown. (b) Results for model II obtained from CS-RPMD (black), MV-RPMD (green), and numerical exact results (red). In this non-adiabatic case, the NRPMD result is close to CS-RPMD and thus is not shown. Magnified plots that correspond to the square regions in both panels are provided on the right-hand side.

results obtained from MV-RPMD (green), CS-RPMD (black), and the numerical exact method (red). As can be seen, the correlation function obtained from MV-RPMD[29] starts to oscillate with a different frequency compared to the quantum result at a longer time. This might happen because the inter-bead couplings for mapping DOF start to contaminate the physical frequency of the system. A similar situation is also encountered in the coherent-state MV-RPMD (result not shown) that samples and propagates trajectories with H_{cmv} [Eq. (A2) in Appendix A]. CS-RPMD, on the other hand, preserves the correct oscillation frequency in the correlation function due to the character of H_{cs} that does not contain the inter-bead coupling for mapping DOF. NRPMD provides a similar result (not shown) compared to CS-RPMD in this non-adiabatic test case. Interestingly, NRPMD and MV-RPMD start to show problematic behaviors at the opposite limit of the electronic coupling, where CS-RPMD provides reliable results across a broad range of parameters as demonstrated in Fig. 1.

Figure 3 presents the nuclear position and the electronic population auto-correlation functions computed from CS-RPMD (black) and the numerical exact method (red) for models IV-VI. Accurately describing electronic interference effects (Rabi oscillations) is essential for non-adiabatic dynamics simulations. Again, CS-RPMD agrees with exact results in the adiabatic regime for model V presented in Fig. 3(a) and provides reasonably good results for the model systems in the intermediate regimes presented in Figs. 3(c)–3(f). The NRPMD approach[34] (results not shown) gives nearly identical results for these correlation functions. MV-RPMD, on the other hand, cannot correctly capture the electronic oscillations in these population auto-correlation functions due to the contamination of the true electronic Rabi oscillations with the inter-beads couplings in the mapping ring-polymer Hamiltonian.[1,29]

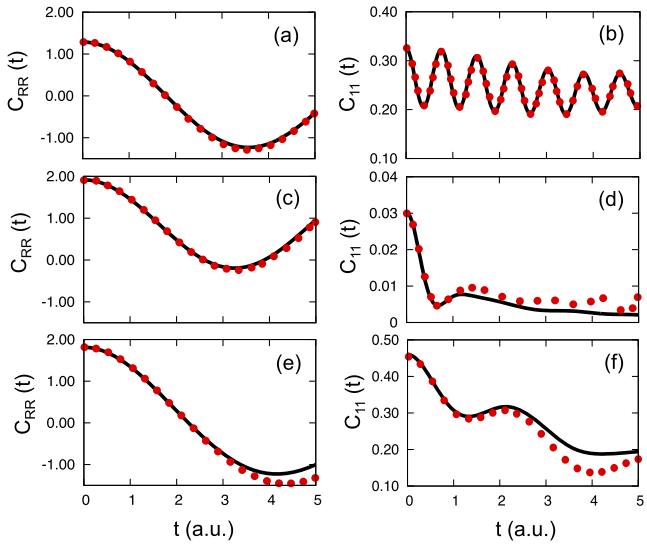

FIG. 3. The Kubo-transformed nuclear position and the electronic population auto-correlation functions for models IV-VI obtained from CS-RPMD (black) and the numerical exact DVR method (red). Results for model V (symmetric, adiabatic) are in panels (a) and (b), model VI (asymmetric, intermediate) are in panels (c) and (d), and model IV (symmetric, intermediate) are in panels (e) and (f).

IV. CONCLUSION

In this paper, we present the CS-RPMD approach, a new state-dependent RPMD method that can accurately describe electronic non-adiabatic dynamics and nuclear quantum effects. With the MMST mapping representation in the coherent-state basis for the electronic DOF and the regular path-integral representation for the nuclear DOF, we derive the CS-RPMD Hamiltonian, which closely resembles the proposed NRPMD Hamiltonian.[34,46] In a special case where there is only one mapping bead (and still multiple nuclear beads), we can rigorously prove that CS-RPMD preserves detailed balance with an approximate quantum Boltzmann distribution. Numerical results from model systems demonstrate the accuracy of this approach across a broad range of electronic coupling regimes.

Compared to recently developed state-dependent RPMD approaches,[29,34] CS-RPMD provides further appealing features, including preserving the electronic Rabi oscillations that MV-RPMD[29] fails to describe. In addition, compared to the NRPMD approach that simply assumes a Hamiltonian of this form,[34] the current work demonstrates how to derive this Hamiltonian from a partition function that contains exact QBD, providing a more solid theoretical foundation for such methods.

The equivalence between RPMD and Kubo-transformed time correlation functions has been originally proposed[24,57] and recently proved through Matsubara dynamics.[46,48,58] We envision a similar rigorous proof[46] of the relation between the CS-RPMD and Kubo-transformed time correlation functions, with a coherent-state mapping Matsubara dynamics framework in future. In addition, we envision to develop a method that exactly preserves both the quantum Boltzmann distribution and the electronic Rabi oscillations and, at the same time, scales linearly with the nuclear DOF and friendly with electronic DOF.[1] Finally, practical directions will focus on applying the CS-RPMD approach to simulate the coupled electron and proton transfer reactions in large-scale condensed phase systems.[25,56]

ACKNOWLEDGMENTS

This work was supported by the University of Rochester startup funds. Computing resources were provided by the Center for Integrated Research Computing (CIRC) at the University of Rochester. We appreciate valuable discussions with Dr. Tim Hele and Professors Tom Miller, Jeremy Richardson, and Nandini Ananth. We appreciate the critical and thorough comments from both reviewers.

APPENDIX A: DERIVATION OF THE COHERENT-STATE MV-RPMD HAMILTONIAN

Here, we obtain the MV-RPMD Hamiltonian in the coherent-state mapping representation. Note that MV-RPMD is not a new method and has been derived in the Wigner basis.[29] We start from the partition function expression in Eq. (2), perform the trace over the electronic DOF with a coherent-state mapping basis, further insert the projection

operator $\mathcal{P} = \sum_n |n\rangle\langle n|$, and arrive at the following expression:

$$\mathcal{Z} \propto \lim_{N\to\infty} \int d\{\mathbf{P}_\alpha\} d\{\mathbf{R}_\alpha\} e^{-\beta_N H_{\rm rp}} \int d\{\mathbf{p}_\alpha\} d\{\mathbf{q}_\alpha\} \times \prod_{\alpha=1}^{N} \langle \mathbf{p}_\alpha, \mathbf{q}_\alpha | \sum_n |n\rangle\langle n| e^{-\beta_N \hat{H}_{\rm e}(\mathbf{R}_\alpha)} | \sum_m |m\rangle\langle m| \mathbf{p}_{\alpha+1}, \mathbf{q}_{\alpha+1}\rangle .$$

The overlap between the diabatic basis and coherent-state basis is explicitly evaluated, and the final expression for coherent-state MV-RPMD partition function is

$$\mathcal{Z}_{\rm cmv} \propto \lim_{N\to\infty} \int d\{\mathbf{R}_\alpha\} d\{\mathbf{P}_\alpha\} d\{\mathbf{q}_\alpha\} d\{\mathbf{p}_\alpha\} {\rm sgn}(\Theta) e^{-\beta_N H_{\rm cmv}} \tag{A1}$$

with the coherent-state MV-RPMD Hamiltonian $H_{\rm cmv}$ defined as

$$H_{\rm cmv} = \sum_{\alpha=1}^{N} \left(\frac{\mathbf{P}_\alpha^2}{2M} + V_0(\mathbf{R}_\alpha) + \frac{M}{2\beta_N^2\hbar^2} (\mathbf{R}_\alpha - \mathbf{R}_{\alpha+1})^2 \right) + \frac{N}{\beta} \sum_{\alpha=1}^{N} \frac{1}{2} (\mathbf{q}_\alpha^{\rm T}\mathbf{q}_\alpha + \mathbf{p}_\alpha^{\rm T}\mathbf{p}_\alpha) - \frac{N}{\beta} \ln|\Theta|. \tag{A2}$$

Here, $\Theta = {\rm Re} \prod_{\alpha=1}^{N} \sum_{nm} [\mathbf{q}_\alpha - i\mathbf{p}_\alpha]_n \mathcal{M}_{nm} [\mathbf{q}_{\alpha+1} + i\mathbf{p}_{\alpha+1}]_m$, with $\mathcal{M}_{nm}(\mathbf{R}_\alpha) = \langle n| e^{-\beta_N \hat{V}_{nm}(\mathbf{R}_\alpha)} |m\rangle$. These results have been derived in the Wigner representation of the mapping variables.[29]

APPENDIX B: MEAN-FIELD RPMD HAMILTONIAN

Here, we derive the mean-field RPMD Hamiltonian with the coherent-state mapping representation. Note that MF-RPMD is not a new method and has been derived without using the mapping representation.[26] Our starting point is the CMV-RPMD partition function expression in Eq. (A1). The mean-field (MF) approximation is applied by integrating over the electronic mapping variables to obtain an effective potential for the nuclear DOF. Analytically evaluating the Gaussian integral over $d\{\mathbf{q}_\alpha\} d\{\mathbf{p}_\alpha\}$ in Eq. (A1), we arrived at the MF-RPMD partition function expression

$$\mathcal{Z}_{\rm MF} \propto \lim_{N\to\infty} \int d\{\mathbf{P}_\alpha\} d\{\mathbf{R}_\alpha\} e^{-\beta_N H_{\rm MF}} {\rm sgn}(\Theta'), \tag{B1}$$

where $H_{\rm MF} = H_{\rm rp} - \frac{N}{\beta} \ln|\Theta'|$ with $\Theta' = {\rm Tr}_{\rm e} \left[\prod_{\alpha=1}^{N} \mathcal{M}(\mathbf{R}_\alpha) \right]$ and $H_{\rm rp}$ is the regular ring-polymer Hamiltonian defined in Eq. (3).

APPENDIX C: RESULTS FOR ONE MAPPING BEAD AND MULTIPLE NUCLEAR BEADS

Figure 4 presents the CS-RPMD results with one mapping bead and eight nuclear beads. Under this special limit, CS-RPMD rigorously preserves detailed balance as $\mathbf{\Gamma}$ becomes an integral of motion of $H_{\rm cs}$. However, CS-RPMD is not able to recover the exact QBD even at t = 0 due to the fact that there is only one bead for mapping DOF and Eq. (10) becomes a rough approximation. As can be clearly seen, the CS-RPMD correlation functions start to deviate from the exact result even at t = 0. Nevertheless, the numerical results of these correlation functions show good agreement with those presented in the main text, suggesting that the nuclear quantization

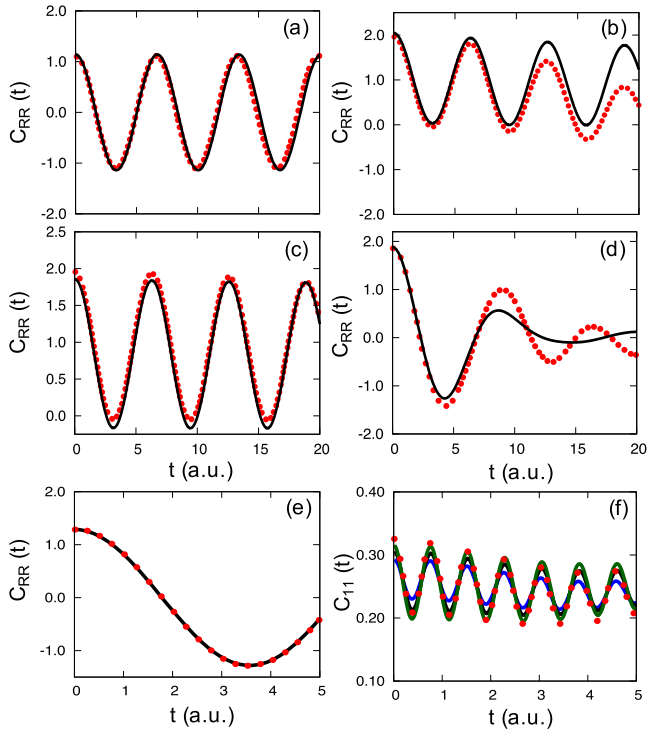

FIG. 4. CS-RPMD correlation functions obtained with one mapping bead and eight nuclear beads. The Kubo-transformed nuclear position auto-correlation functions for models I-IV are presented in (a)–(d), and the Kubo-transformed nuclear position and population auto-correlation functions for model V are presented in (e) and (f). Results are obtained from CS-RPMD (black) and the numerical exact DVR method (red). For the population auto-correlation function presented in (f), CS-RPMD results are obtained with one mapping bead and 1 (blue line), 8 (black line), and 16 (green line) nuclear beads.

is the most important factor for achieving an accurate result in these test cases. Thus for the calculations presented here, we expect that the MMST Hamiltonian (which appears under this one mapping bead limit) is accurate for describing non-adiabatic effects, and nuclear quantization with ring-polymer should be able to capture the nuclear quantum effects, leading to a reasonable numerical accuracy.

[1] S. C. Althorpe, N. Ananth, G. Angulo, R. D. Astumian, V. Beniwal, J. Blumberger, P. G. Bolhuis, B. Ensing, D. R. Glowacki, S. Habershon, S. Hammes-Schiffer, T. J. H. Hele, N. Makri, D. E. Manolopoulos, L. K. McKemmish, T. F. Miller III, W. H. Miller, A. J. Mulholland, T. Nekipelova, E. Pollak, J. O. Richardson, M. Richter, P. R. Chowdhury, D. Shalashilin, and R. Szabla, Faraday Discuss. **195**, 311 (2016).
[2] J. Tully, J. Chem. Phys. **93**, 1061 (1990).
[3] J. E. Subotnik, A. Jain, B. Landry, A. Petit, W. Ouyang, and N. Bellonzi, Annu. Rev. Phys. Chem. **67**, 387 (2016).
[4] L. Wang, A. Akimov, and O. V. Prezhdo, J. Phys. Chem. Lett. **7**, 2100 (2016).
[5] D. M. Kernan, G. Ciccotti, and R. Kapral, J. Phys. Chem. B **112**, 424 (2008).
[6] H. Kim, A. Nassimi, and R. Kapral, J. Chem. Phys. **129**, 084102 (2008).
[7] C. Hsieh and R. Kapral, J. Chem. Phys. **137**, 22A507 (2012).
[8] C. Hsieh and R. Kapral, J. Chem. Phys. **138**, 134110 (2013).
[9] R. Kapral, J. Phys.: Condens. Mat., **27**, 073201 (2015).
[10] W. H. Miller, J. Phys. Chem. A **105**, 2942 (2001).
[11] W. H. Miller, J. Phys. Chem. B **113**, 1405 (2009).
[12] X. Sun, H. Wang, and W. H. Miller, J. Chem. Phys. **109**, 7064 (1998).
[13] Q. Shi and E. Geva, J. Phys. Chem. A **108**, 6109 (2004).
[14] P. Huo and D. F. Coker, J. Chem. Phys. **135**, 201101 (2011).
[15] J. C. Tully, J. Phys. Chem. Lett. **137**, 22A301 (2012).
[16] J. Liu and W. H. Miller, J. Phys.: Condens. Matter **27**, 073201 (2015).
[17] P. V. Parandekar and J. C. Tully, J. Chem. Theory Comput. **2**, 229 (2006).

[18]J. R. Schmidt, P. V. Parandekar, and J. C. Tully, J. Chem. Phys. **129**, 044104 (2008).
[19]U. Muller and G. Stock, J. Chem. Phys. **111**, 77 (1999).
[20]S. Habershon and D. E. Manolopoulos, J. Chem. Phys. **131**, 244518 (2009).
[21]J. Cao and G. Voth, J. Chem. Phys. **100**, 5106 (1994).
[22]S. Jang and G. Voth, J. Chem. Phys. **111**, 2371 (1999).
[23]S. Habershon, D. E. Manolopoulos, T. E. Markland, and T. F. Miller, Annu. Rev. Phys. Chem. **64**, 124105 (2013).
[24]I. R. Craig and D. E. Manolopoulos, J. Chem. Phys. **121**, 3368 (2004).
[25]A. R. Menzeleev, N. Ananth, and T. F. Miller, J. Chem. Phys. **135**, 074106 (2011).
[26]T. J. H. Hele, "An electronically non-adiabatic generalization of ring polymer molecular dynamics," MChem thesis, Exeter College, University of Oxford, 2011.
[27]J. R. Duke and N. Ananth, Faraday Discuss. **195**, 253 (2016).
[28]A. R. Menzeleev, F. Bell, and T. F. Miller, J. Chem. Phys. **140**, 064103 (2014).
[29]N. Ananth, J. Chem. Phys. **139**, 124102 (2013).
[30]J.-L. Liao and G. A. Voth, J. Phys. Chem. B **106**, 8449 (2002).
[31]P. Shushkov, R. Li, and J. C. Tully, J. Chem. Phys. **137**, 22A549 (2012).
[32]F. A. Shakib and P. Huo, J. Phys. Chem. Lett. **8**, 3073 (2017).
[33]T. Yoshikawa and T. Takayanagi, Chem. Phys. Lett. **564**, 1 (2013).
[34]J. O. Richardson and M. Thoss, J. Chem. Phys. **139**, 031102 (2013).
[35]H. D. Meyer and W. H. Miller, J. Chem. Phys. **70**, 3214 (1979).
[36]G. Stock and M. Thoss, Phys. Rev. Lett. **78**, 578 (1997).
[37]M. Thoss and G. Stock, Phys. Rev. A **59**, 64 (1999).
[38]R. P. Feynman and A. R. Hibbs, *Quantum Mechanics and Path Integrals* (Dover Publications, Inc., 1965).
[39]B. J. Berne and D. Thirumalai, Annu. Rev. Phys. Chem. **37**, 401 (1986).
[40]D. M. Ceperley, Rev. Mod. Phys. **67**, 279 (1995).
[41]D. Chandler and P. G. Wolynes, J. Chem. Phys. **74**, 4078 (1981).
[42]M. H. Alexander, Chem. Phys. Lett. **347**, 436 (2001).
[43]J. R. Schmidt and J. C. Tully, J. Chem. Phys. **127**, 094103 (2007).
[44]N. Ananth and T. F. Miller, J. Chem. Phys. **133**, 234103 (2010).
[45]J. Lu and Z. Zhou, J. Chem. Phys. **146**, 154110 (2017).
[46]T. J. H. Hele and N. Ananth, Faraday Discuss. **195**, 269 (2016).
[47]P. Huo, T. F. Miller, and D. F. Coker, J. Chem. Phys. **139**, 151103 (2013).
[48]T. J. H. Hele, M. J. Willatt, A. Muolo, and S. C. Althorpe, J. Chem. Phys. **142**, 134103 (2015).
[49]S. Bonella and D. Coker, J. Chem. Phys. **114**, 7778 (2001).
[50]S. Bonella and D. Coker, J. Chem. Phys. **118**, 4370 (2003).
[51]W. H. Miller and S. J. Cotton, Faraday Discuss. **195**, 9 (2016).
[52]S. J. Cotton and W. H. Miller, J. Phys. Chem. A **119**, 12138 (2015).
[53]J. Liu, J. Chem. Phys. **145**, 204105 (2016).
[54]J. O. Richardson, P. Meyer, M.-O. Pleinert, and M. Thoss, Chem. Phys. **482**, 124 (2017).
[55]D. T. Colbert and W. H. Miller, J. Chem. Phys. **96**, 1982 (1992).
[56]J. S. Kretchmer and T. F. Miller, J. Chem. Phys. **138**, 134109 (2013).
[57]B. J. Braams and D. E. Manolopoulos, J. Chem. Phys. **125**, 124105 (2006).
[58]T. J. H. Hele, M. J. Willatt, A. Muolo, and S. C. Althorpe, J. Chem. Phys. **142**, 191101 (2015).